THE ASTROPHYSICAL JOURNAL, 229:274–290, 1979 April 1

APPLICATION OF LINE TRANSFER CALCULATIONS TO ACTIVE NUCLEI AND NOVAE

GARY FERLAND*
AND
HAGAI NETZER†
McDonald Observatory and Department of Astronomy, University of Texas at Austin
Received 1978 June 8; accepted 1978 September 29

ABSTRACT

We apply Monte Carlo calculations to realistic nebulae in order to study the effects of internal dust and level-2 population on the observed spectrum. We show that severe Lα trapping is obtained in all cases, and penetration of line photons to optical depths as large as 10^7 is common. We use photoionization calculations to mimic the photon generating function in quasars and other gaseous nebulae, and show that level-2 population is concentrated deep in the cloud, due to trapping and some collisional excitation of Lα. We calculate the Balmer optical depth and give simple formulae to deduce it in different situations. The optical depth $\tau_{H\alpha}$ can reach a very large value, but an effective optical depth 8–15 times smaller must be used when calculating Balmer self-absorption. We use our results to study the collisional excitation of Balmer lines, the level-2 ionization by Lα, and thermalization. The last cannot amount to more than ~30% destruction of Lα under typical active nuclei conditions ($N_e < 10^{10}$ cm^{-3}) and cannot therefore explain the anomalous observed Lα/Hβ. We study the destruction of Lα and some metallic lines like C IV λ1549 in nebulae containing dust, and give their destruction as a function of both the dust and the line optical depths. Severe destruction of Lα can occur, but observed line ratios like He II λ1640/Lα suggest that the amount of internal dust in QSOs is small; and if it is the only attenuation mechanism, then Lα/Hβ $\gtrsim$ 15. External dust may be more important. Synthetic QSO spectra are shown for cases of internal dust with different dust/gas ratios. In an appendix we apply some results to novae, and show that they can nicely explain the observed Hα/Hβ and O I λ8446 in V1500 Cygni. The calculations demonstrate the importance of using realistic ionization structure and dust properties in investigating line trapping and destruction.

Subject headings: galaxies: nuclei — quasars — radiative transfer — stars: novae

I. INTRODUCTION

This paper discusses several aspects of resonance line transfer in gaseous nebulae. Previous attempts along this line have concentrated on the Lα transfer, with some simplified assumptions about the photon generating function (like uniform generation). In realistic situations the line generating function depends on the ionizing continuum and thus differs from one case to another.

In this work we combine realistic ionization structures (for both blackbody and power-law continuum sources) with the Monte Carlo line transfer technique, to study the line trapping and level-2 population for astrophysically important cases. We use our calculations to investigate in detail questions like the destruction of resonance lines by internal dust, the Balmer lines optical depths, and the thermalization of Lα.

The following section describes the method and details of our calculations. Section III discusses the case of dust-free nebulae, while § IV includes the effect of dust and thermalization. Finally, in § V we apply our results to active nuclei. Some examples and applications to novae and other gaseous nebulae are given in an appendix.

II. METHOD

We considered cases of gaseous nebulae ionized by a radiation from a central object. Continuum ionizing photons penetrate to optical depths $\gtrsim$10, so Lα photons are created at line center optical depths of $\tau_0 \geq 10^5$ (for thermal broadening). Since thermalization (collisional de-excitation) of strong resonance lines is unlikely for typical nebular densities ($N_e < 10^{10}$ cm^{-3}), these photons will scatter many times before eventually escaping from the nebula. The diffusion process is dominated by the frequency shifts that occur during the scattering because it is much more likely that a photon will escape after a shift into the line wings (where the nebula is optically thin), than by a gradual random walk out of the cloud (Osterbrock 1962). The frequency redistribution function must therefore be treated exactly. Standard analytic line transfer techniques (Jefferies 1968; Mihalas

* Now at the Institute of Astronomy, Cambridge, England.
† On leave from the Department of Physics and Astronomy, Tel Aviv University.

1970) do not incorporate complicated redistribution functions, so Monte Carlo methods are often employed (Auer 1968; Avery and House 1968).

In this paper, we shall consider only plane-parallel geometry which seems to be the best approximation of many realistic cases where the matter is distributed in clumps or very thin shells (like QSO emission regions). Such a geometry was assumed in the calculations of Auer (1968) and Avery and House (1968). Panagia and Ranieri (1973*a*) have considered the alternative static spherical envelope case.

The equation of transfer takes the familiar form

$$\mu \frac{dI(X)}{d\tau(X)} = I(X) - S(X)\,, \tag{1}$$

where the source function is

$$S(X) = \frac{(1-\epsilon)}{\phi(X)} \int_{-\infty}^{\infty} R(X', X) J(X') dX' + G\,. \tag{2}$$

Here $R(X', X)$ is the probability of the photon receiving a shift from frequency X' (in units of the Doppler width) to X, J is the mean intensity, and $4\pi G$ is the rate at which photons are created by both collisional processes and recombination. The quantity ϵ represent losses due to all destruction processes which for Lα is mainly the relative collisional de-excitation rate, and $\phi(X)$ is the Voigt function. The ratio of damping width to Doppler width, $a = \Gamma/4\pi\Delta\nu_D$, is 4.7×10^{-4} for hydrogen Lα at 10^4 K, and is the value used for all the calculations in this paper.

Two types of frequency redistribution are possible. In the high-density limit ($N_e \gg 10^{13}$ cm^{-3}), the emitted and absorbed frequencies are entirely uncorrelated since the atom is perturbed between emission and absorption. In this case, the redistribution function can be written as

$$R(X', X) = \phi(X')\phi(X)\,. \tag{3}$$

This *complete* redistribution function was considered by Avery and House (1968) and by Panagia and Ranieri (1973*a*). In the low-density limit, scattering is coherent in the frame of the atom, but incoherent in the external frame because of Doppler shifts due to the thermal motions of the emitters. This case has been considered by Spitzer (1944), Unno (1952), and Osterbrock (1962), and by the Monte Carlo calculations of Auer (1968), Avery and House (1968), and Bonilha, Ferch, and Salpeter (1979). The redistribution function takes the more complicated form (Unno 1952)

$$R(X, X') = \delta_{XX'} \Big/ \int_{-\infty}^{\infty} \delta_{XX'} dX\,, \tag{4}$$

where

$$\delta_{XX'} = \frac{1}{\pi^{3/2}} \int_{(x_l - x_s)/2}^{\infty} \exp(-\zeta^2) \left(\tan^{-1} \frac{\zeta - x_l}{a} + \tan^{-1} \frac{\zeta + x_s}{a} \right) d\zeta\,, \tag{5}$$

where x_l is the larger and x_s is the smaller of the pair (X, X'). This *partial* redistribution function has been plotted by Osterbrock (1962) and by Avery and House (1968).

The choice of either redistribution function does not affect the transfer problem when $\tau_0^{\rm tot} < 10^4$ since the escaping photons have frequencies near the core. Order-of-magnitude differences in the mean number of scattering result if $\tau_0^{\rm tot} > 10^5$ (Avery and House 1968) since the probability of a shift into the far line wings, P, is much larger for complete redistribution ($P \propto X^{-2}$ for the damping wings) than for partial redistribution ($P \propto e^{-X^2}$ since the photon receives a large shift only if it is absorbed by an atom moving with a large velocity). Models with both redistribution functions will be computed here, but partial redistribution probably best describes the scattering process in ejecta from novae, the nuclei of active galaxies, and many other cases of interest where $N_e \ll 10^{13}$ cm^{-3}.

We will only describe briefly the Monte Carlo technique which is well described in the literature (Auer 1968; Avery and House 1968; Panagia and Ranieri 1973*a*). A detailed description of our program is presented elsewhere (Ferland 1978*b*). The technique assumes that the transfer process can be treated photon by photon (which is the case for Lα in nebular conditions where $N_2/N_1 \ll 1$.) After a photon is created at a given position within the slab, the computer's random number generator is used to choose a frequency and direction, and the photon is advanced to the new position using the path length found. In each step the relevant probability functions are sampled to test for destruction by dust or thermalization, and the process is continued until the photon either escapes or is destroyed. A core approximation was employed for frequencies smaller than 2.1 Doppler widths at optical depths greater than 10^3. This common approximation treats the numerous scatterings at small Doppler widths analytically since the photon is likely to move only a slight distance during these scatterings. A special technique was developed to adequately sample in frequency between 0 and 30 Doppler widths, using only 300 cells. Check runs were performed and gave good agreement with calculations of the mean number of scattering by Auer (1968) and Avery and House (1968).

Of prime importance is the generating function, $G(\tau)$, which gives the probability of creating a photon at an optical depth τ in the line center. Earlier attempts to apply the Monte Carlo technique to astrophysically important cases used too simplified $G(\tau)$. For example, Auer (1968) has considered the Lα transfer assuming evenly distributed emitters, while Avery and House (1968) have placed all the emitters at the center of the slab. Panagia and Ranieri (1973*a*) assert that a generating function proportional to r^{-2} will mimic a Strömgren sphere. (Actually in physical space the generating function is proportional to N_e^2 and is nearly constant across a blackbody Strömgren sphere). As far as we know, no attempt has been made to consider lines other than Lα.

We have used photoionization model calculations to obtain the generating function for realistic nebulae. The computer program used in the calculation is described in Baldwin and Netzer (1978). It involves standard techniques of solving for the ionization and thermal equilibrium at every point of the slab and then uses these to obtain the line intensities. Constant pressure cases are usually assumed. Models with both blackbody and power-law ionization radiation fields were computed and chosen to closely mimic conditions in typical active nuclei, novae, and H II regions. The emissivity and the ionization structure as calculated at many points across the slab are used to obtain the generating functions as well as the optical depth for the different lines of interest. In what follows, we give optical depths assuming turbulent velocities of 20 km s^{-1} for all lines. The resulting τ_0 is slightly underestimated for Lα and by a factor of ~ 5 for heavier elements, compared with the pure thermal case. The actual internal velocity depends on the dynamics of individual cases, which we shall not discuss here.

Our plan of attack is as follows. The generating function can be computed from our model ionization structure since that structure is independent of the line transfer. Equations (1) and (2) are then solved, using the Monte Carlo method. The problem is simplified since the continuum transfer solution is totally decoupled from the line transport solution. We assume that ionization and other depopulation processes of level-2 are negligible. This will be justified in § IV.

III. DUST-FREE CASES

a) Uniform Generation

A set of models was computed with photons created uniformly across a slab of thickness τ_0. These cases are important since we found that most of the strong metallic lines in active nuclei and novae (C IV λ1549, O VI λ1035, Mg II λ2798, etc.) have nearly uniform generating function (see § IV). Figure 1 shows both $\langle N \rangle$, the mean number of scatterings, and $\langle P \rangle$, the mean path traversed, as functions of the total slab thickness for these cases.

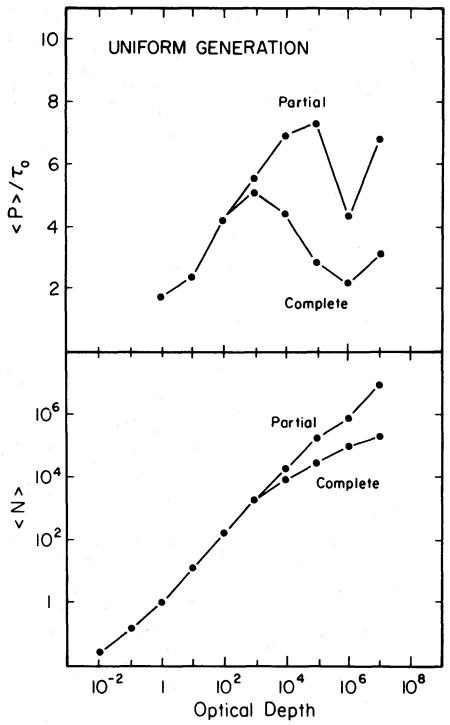

FIG. 1.—Mean number of scattering $\langle N \rangle$, and path traveled $\langle P \rangle / \tau_0$, as a function of the total slab optical depth in a uniform generation case. Estimated uncertainty is $\pm 10\%$. The dip at $\tau \sim 10^6$ was also seen by Avery and House (1968). The partial redistribution case is a good representation of many metallic resonance lines in QSOs and novae.

The largest optical depth for which Monte Carlo calculations have been reported previously was $\tau_0 = 10^5$ (Auer 1968; Avery and House 1968). Analytic techniques were used to estimate $\langle N \rangle$ for larger optical depths by Osterbrock (1962), Avery and House (1968), and Adams (1972). Osterbrock and Avery and House both found a nearly linear ($\langle N \rangle$, τ_0)-relationship for $\tau_0 < 10^5$. At larger τ_0 Osterbrock found $\langle N \rangle \propto \tau_0^2$, but Avery and House found that the linear dependence continued at least until 10^7. Hummer and Rybicki (1971) remarked that the large τ_0 situation was unclear. Adams has shown that the linear dependence holds up to $\tau_0 = 10^8$ and has provided a physical explanation for the discrepancy. Our numerical results confirm Adams's finding that the linear dependence is continued past $\tau_0 = 10^7$. This is also in accordance with recent calculations by Bonilha, Ferch, and Salpeter (1979).

We have fitted the ($\langle N \rangle$, τ_0)-curve (for partial redistribution) with the relation

$$\langle N \rangle = 1.11\tau_0^{0.826} \quad (\tau_0 < 1)$$

$$= \frac{1.11\tau_0^{1.071}}{1 + (\log_{10}\tau_0/5.5)^5} \quad (\tau_0 \geq 1). \tag{6}$$

These expressions are as accurate as the Monte Carlo calculations ($\sim 15\%$ at most optical depths). The dip at $\tau_0 = 10^6$, which was also found by Avery and House, is not reproduced by these formulae. The mean escape probability is given by $(1 + \langle N \rangle)^{-1}$. The shape of the ($\langle P \rangle$, τ_0)-curve is similar to that found by Bonilha, Ferch, and Salpeter (1979), but specific values differ because different generating functions were used.

b) Lα *in Gaseous Nebulae*

We have run models to mimic the Lα transfer in nebulae ionized by three radiation sources: two nonthermal (with different slopes) and a blackbody. Table 1 summarizes the details of the models, and Figure 2 shows the three generating functions, all very different from a uniform case.

The difference between the generating functions shown is mainly due to the different contribution of Lα(coll) (Lα excited by collisions from the ground state) to the source function. This contribution can amount to more than half of the total flux in the line, in cases of flat nonthermal continuum and small ionization parameter U_1 ($U_1 = F_1/N_{\rm H}h$, where F_1 is the incident flux at 1 rydberg). It is caused by penetration of high-energy photons deep into the cloud, where a low-ionization, high-temperature ($\sim 10{,}000$ K) region is formed in which Lα(coll) is the strongest line. All the generating functions shown are flat up to $\tau_{\rm L\alpha} \sim 10^4$ (they depend on $N_e^2/N_{\rm H}$, and the ionization is constant), where they start to drop, and the slope of their remaining part depends on the amount of Lα(coll). In all cases of a very steep nonthermal continuum or large U_1, where the H^+ layer is thick enough to absorb all high-energy photons, the only contribution to Lα is due to recombination and we get a single curve (Fig. 2*c*). This curve represents also all blackbody continua over a large range in temperature since the ionizing continuum is too steep to excite an appreciable amount of Lα(coll). Note here that we only consider blackbodies with small dilution factors. It seems that most cases of interest can be reduced to the three curves shown in Figure 2, and differences between all cases with *no* Lα(coll) are negligible. An example of line emissivities across a QSO cloud is shown in Figure 3, and detailed calculation of Lα(coll) in other cases can be found in Baldwin and Netzer (1978).

The rather large number of scatterings presented in Table 1 may appear surprising since the majority of the photons are created at optical depth $\leq 10^5$. The reason is that some of the photons penetrate deep into the cloud and contribute most of the scatterings. To demonstrate this, we show in Figure 4 a test case in which photons were created uniformly between $0 < \tau_0 < 10^3$, and the outer edge of the slab was moved to larger and larger optical depth $\tau_0^{\rm tot}$ and acts *only to reflect* the photons (i.e., all material beyond $\tau_0 = 10^3$ is neutral). Two curves, representing the mean number of scatterings and the percentage of photons escaping in the outward direction,

TABLE 1

Hα Optical Depth

Model	U_1(cm s^{-1})	η	β	$\langle N \rangle$*
a) Power law $\nu^{-0.8}$.....	$< 1.5 \times 10^8$	3.0	1.9×10^{-15}	$(3.8 \pm 0.7) \times 10^6$
b) Power law $\nu^{-1.6}$.....	$< 2 \times 10^8$	2.0	7.2×10^{-16}	$(1.4 \pm 0.3) \times 10^6$
c) All power laws.....	$> 10^9$	1.0	6.6×10^{-16}	$(1.3 \pm 0.3) \times 10^6$
d) All blackbody.....	All	1.0	6.6×10^{-16}	$(1.3 \pm 0.3) \times 10^6$

* $\langle N \rangle$ is the mean number of scatterings of Lα (partial redistribution). Hα optical depth obtained from $\tau_{\rm H\alpha} = \eta\beta[Q({\rm H})/4\pi r^2]V_{20}^{-2}$, where Q(H) is the number of ionizing photons, r the distance from the central source in cm, and V_{20} the turbulent velocity in 20 km s^{-1}. The uncertainty of β is the same as for $\langle N \rangle$. The quantity η is calculated from the model photoionization, and can change by up to 20% according to the value of U_1. Note that the "effective $\tau_{\rm H\alpha}$," as described in the text, is 8–15 times smaller, and is a better one to use in self-absorption calculations. The equivalent complete redistribution case gives ~ 20 times fewer scatterings.

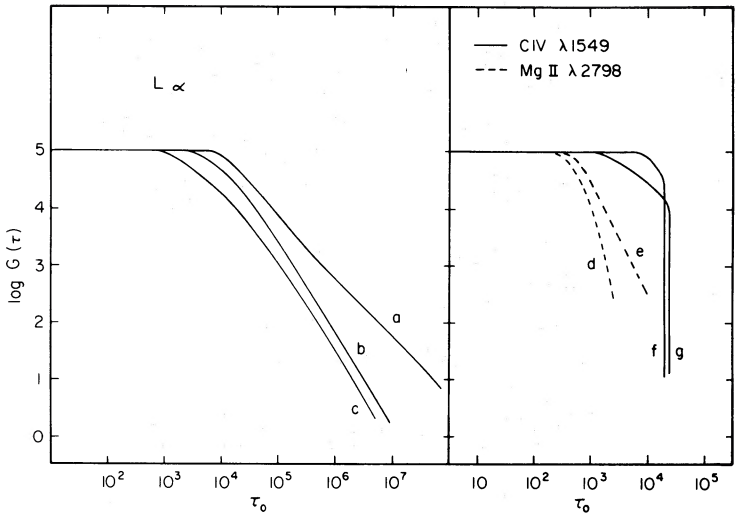

FIG. 2.—Different realistic generating functions (emissivity per unit optical depth) as calculated in this work. (*a*) Lα for a $\nu^{-0.8}$ continuum with large fraction of Lα(coll) ($U_1 \lesssim 1.5 \times 10^8$ cm s^{-1}). (*b*) A $\nu^{-1.6}$ continuum with large fraction of Lα(coll) ($U_1 \lesssim 3 \times 10^8$ cm s^{-1}). (*c*) All nonthermal continuum with small fraction of Lα(coll) ($U_1 > 10^9$ cm s^{-1}). All blackbody, all cases with dust for powerlaw and blackbody continua. (*d*) Mg II λ2798 with large amount of dust [τ_d(eff) ≈ 0.6]. (*e*) Mg II λ2798 with small amount of dust [τ_d(eff) ≈ 0.1]. (*f*) C IV λ1549 for most nonthermal and blackbody cases with small amount of dust, and with no dust. Also representing lines of O VI λ1035, Si IV λ1397, N V λ1240, etc., with an appropriate scaling of optical depth. (*g*) C IV λ1549 for nonthermal continuum and large amount of dust [τ_d(eff) ≈ 0.6].

are shown. As the total slab thickness increases, the mean number of scatterings increases, and the fraction of the photons escaping in the outward direction decreases. For the largest τ_0^{tot} considered, no photons escape in the outward direction, and the mean number of scatterings increases by a factor of 40. This points out the danger of considering only a single characteristic optical depth in solving the transfer problem. It also reemphasizes the difference between the cases discussed in this work, and the uniform generation considered in the past.

All of our models were radiation bounded (outer edge of the shell occurs where the ionizing flux is extinguished),

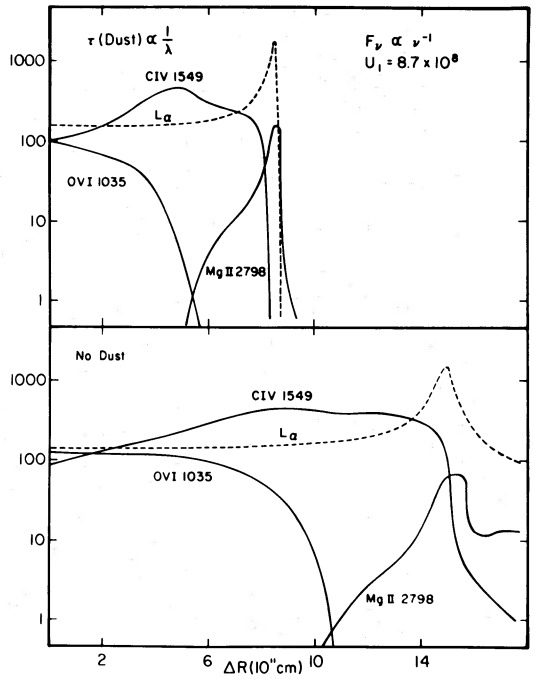

FIG. 3.—The emissivity of different emission lines across a QSO cloud near a $F_\nu \propto \nu^{-1}$ continuum. The dusty case shown has $\tau_d(912) = 0.14$ corresponding to dust/gas ≈ 0.1 galactic. The peak in the Lα curve is due to Lα(coll) which, in the dusty case, is reduced in total intensity by ~85%. The integrated spectrum of this model is given in Table 3.

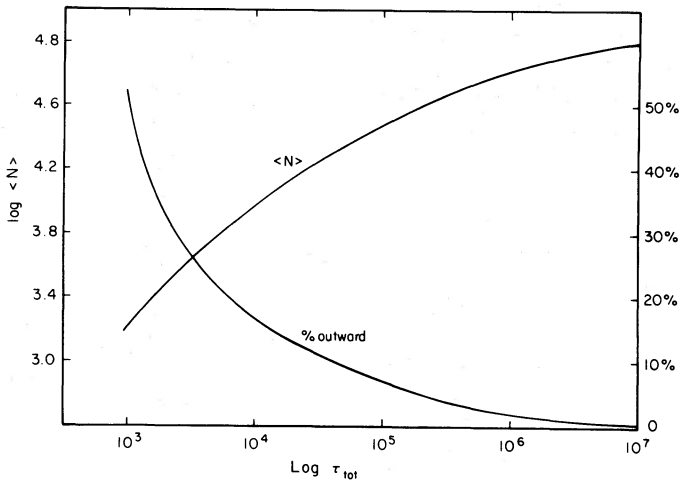

FIG. 4.—In this example, photons were created uniformly across a slab of thickness $\tau_0 = 10^3$. A second region, in which photons were not created, but were merely allowed to scatter, was placed at one edge of the generating region, and the optical depth of this second region was increased. This mimics the situation with Lα, since photons are usually created at $\tau_0 < 10^5$, but optical depths as great as 10^7 are heated significantly. As the optical depth of the second region increases, the mean number of scatterings also increases, but the fraction of the photons that escape through the second region decreases.

and the maximum optical depth of $\tau_{L\alpha} = 10^7$ is beyond the point where 99% of the Lα photons were created. An important consideration related to this, which is often overlooked, is that the Lα optical depth in a Strömgren sphere is *not* a free parameter. Since the ratio $K_0(L\alpha)/K_\nu(912)$ is $\sim 10^4$ for thermal motion, the majority of recombinations occur at Lα optical depths $\tau(L\alpha) < 10^5$, although material as deep as 10^7 can be heated significantly in some cases, as described. The neutral hydrogen beyond the heated region does not affect the transfer of Lα photons since the vast majority of them escape through the inner surface of the Strömgren sphere, without reaching that region at all.

Our Monte Carlo calculations ignore the variation in Doppler width of Lα (due to changes in T_e) across the Strömgren shell. This is not a serious problem since the effects of this change tend to cancel one another. If the line broadening is actually larger than we assume, then Lα will have a smaller optical depth at line center (which will decrease the number of scatterings), but the damping constant will also be smaller (which tends to increase the number of scatterings). Also we did not consider cases with internal expansion.

c) *Level-2 Population*

We have calculated the distribution of H^0 atoms in the first excited state to enable calculation of the optical depth in the hydrogen Balmer lines. The balance equation for the *two-level* atom is

$$N_2(C_{21} + A_{21}) = N_1\left(C_{12} + K\int \phi_\nu J_\nu d\nu\right) + N_e{}^2\alpha_2{}^{\rm eff}\,, \tag{7}$$

where the term on the left represents processes which depopulate level-2 (collisional and radiative de-excitation) and the right-hand side represents processes that populate level-2 (collisional excitation, radiative excitation [the most important], and recombination). Other terms of similar type should be added when transitions to and from more levels are included. The ratio of collisional to radiative de-excitation will be

$$\epsilon = \frac{C_{21}}{A_{21}} = \frac{N_e q_{21}}{A_{21}}\,. \tag{8}$$

For Lα this is of order of $10^{-16.7} N_e$. Collisional de-excitation or thermalization will be unimportant when $\epsilon\langle N_{\rm scat}\rangle \ll 1$. For the majority of the calculations presented in this paper collisional de-excitation was neglected (a good assumption when $N_e < 10^9$ cm^{-3}). Some calculations with thermalization of the photon will be presented in § IV.

The level-2 population is a simple by-product of our calculation. An array of counters was placed through the slab, and were used to record the number of times photons were scattered at given positions. The Hα optical depth is given by

$$\tau_{H\alpha} = \frac{\langle N_{\rm scat}\rangle}{A_{21}} K_{H\alpha} Q_{\rm eff}\,, \tag{9}$$

where $\langle N_{scat} \rangle$ is the mean number of scatterings of Lα, $K_{H\alpha}$ is the opacity of Hα (3.2×10^{-13} cm^2 for $V = 20$ km s^{-1}), and Q_{eff} is the number of photons created that populate level 2 per unit time and area. (In other words, $\langle N_{scat} \rangle Q_{eff}/A_{21}$ gives the level-2 column density.)

For a radiation-bounded Strömgren sphere, located a distance R from the central object,

$$Q_{eff} = \frac{\int_1^\infty (F_\nu/h\nu) d_\nu}{4\pi R^2} \eta \equiv \frac{Q(\mathrm{H})}{4\pi R^2} \eta , \tag{10}$$

which is the number of photons capable of ionizing hydrogen which are intercepted by the nebula, per unit area and time, multiplied by a factor to account for thermal excitation, $\eta = 1 +$ coll/recb. The quantity η is quite model dependent, but is usually within the range $1 < \eta < 3$. We shall give η and the constant

$$\beta = \frac{\langle N_{scat} \rangle K_{H\alpha}}{A_{21}} \tag{11}$$

in the equation

$$\tau_{H\alpha} = \beta Q_{eff} \tag{12}$$

for the models we consider. Note that this gives the total Hα optical depth, and is not the best value to use for mean escape probability calculations (see § V).

Figure 5 shows the generating function and level-2 population corresponding to one of the models (Fig. 2*c*). The line generating function is more strongly peaked to the interior of the cloud than is the distribution of level-2 populations (i.e., most of the Balmer opacity is deep in the cloud, while most of the photons are created near the ionized surface) because photons created near the inner boundary of the slab can penetrate to large optical depths. This distribution will affect the symmetry of Balmer emission lines in expanding envelopes since Balmer photons will be more likely to escape through the inner boundary (Ferland, Netzer, and Shields 1979).

IV. DESTRUCTION PROCESSES

a) Internal Dust

We consider first several astrophysically important situations, where dust is mixed with the gas, causing destruction of line photons. We discuss cases of constant dust-to-gas ratio across the cloud, and different dust properties. The model requires two separate sets of calculations—one to investigate changes in the photon generating function (i.e., the influence of dust on the ionizing radiation field) and the other to calculate the destruction of different lines due to the multiscattering process.

A main cause of concern in such calculations is the unknown dust properties for $\lambda < 912$ Å. Study of the interstellar extinction curve gives some clues to the grain distribution (Mathis, Rumple, and Nordsieck 1977), but different types of grains may be responsible for absorption at shorter wavelength, on which we do not have any information. Studies in our own Galaxy (Mezger, Smith, and Churchwell 1974; Chaisson, Lichten, and Rodriguez

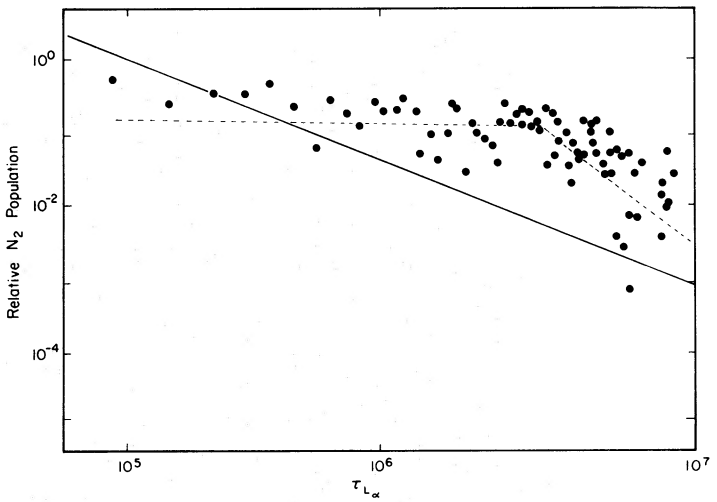

FIG. 5.—Level-2 population. The slab is divided into 100 parts, each of optical depth 10^5, and the number of scatterings within each subslab is saved, and is presented here as the mean number of scatterings per unit optical depth, per created photon. This is proportional to N_2/N_1. This example is for a blackbody generating function (Fig. 2*c*) and only 100 photons. The generating function is shown as the solid line, and is more strongly peaked toward the inner surface of the slab than is the level-2 population (which is linearly related to $\langle N \rangle$).

1978) suggest an extinction that varies between $1/\lambda$ and $1/\lambda^2$ for $\lambda < 912$ Å. On the other hand, theoretical calculations give a much slower variation with wavelength, perhaps even a constant cross section (e.g., Aannestad 1975). Obviously dust near QSOs may be of different composition. Also it may be subjected to destruction processes, destroying part or all particles, at different distances from the powerful central source. Considering this, we have tried a variety of models with different assumptions about the dust properties.

We define an effective optical depth by

$$\tau_d(\text{eff}) = (1 - \bar{a})\tau_{\text{dust}}, \tag{13}$$

where $\bar{a}$ is the albedo and τ_{dust} is the total dust optical depth. It fixes the fraction of the ionizing radiation removed by the dust, and stands for different combinations of albedo and extinction. We shall use $\tau_d(\lambda)$ to stand for the value of τ_d(eff) at λ, and measure it for all lines at the point where 99% of the photons were created. In this way different lines, with different emission zones, will also have different τ_d(eff). Cases tried are $\tau_d(\text{eff}) \propto 1/\lambda$ and $\tau_d(\text{eff}) \propto 1/\lambda^2$, but we consider the first to be more realistic and use it in the cases to follow. For comparison purposes we have extrapolated the interstellar extinction curve to get:

$$A_{912\text{Å}} = 2 \times 10^{-21} \times (\text{H column density}) \text{ mag}. \tag{14}$$

We refer to this as representing a "galactic" dust/gas ratio. A complete forward scattering by the dust is assumed, close to what was found for the interstellar dust at $\lambda \approx 1500$ Å (Lillie and Witt 1976). Most of our results are not very sensitive to this assumption within the range of τ_d(eff) chosen (Baldwin and Netzer 1978), and the only case where this may be significant is discussed later on.

The photoionization program described earlier was modified to include the effect of internal dust. A detailed description of such calculations is given by Baldwin and Netzer (1978), who investigated the effects of internal dust on the ionization of QSO clouds. Here we summarize their most important results related to the present study.

The main effect of dust with the above properties is to cut the number of high energy photons and thus affecting Lα(coll) and several other lines. The reason is that the dust reduces considerably the transition zone (§ III) where the emission of Lα(coll) and low-excitation lines like Mg II λ2798 takes place, even for very low values of τ_d(eff). An example is shown in Figure 3, where the emissivity of different lines is compared with a dust-free case, for a QSO cloud near an $F_\nu \propto \nu^{-1}$ continuum. In this case, the dust/gas ratio is 10 times smaller than the galactic value, $\tau_d(\text{eff}) \propto 1/\lambda$ and $\tau_d(912\text{ Å}) \approx 0.14$. Even such a small amount is enough to destroy ~85% of Lα(coll) while the recombination part of the line drops only by ~30%. [Note that Lα(coll) is the peak in the Lα curve.] The high-excitation lines, like O VI λ1035, are also strongly affected by the depletion of high energy photons.

Baldwin and Netzer (1978) concluded that the above behavior is very typical in most cases of small τ_d(eff) regardless of the exact dependence of τ_d(eff) on wavelength. Among the lines we are interested in, Lα is affected most. We have compared several nonthermal continua ($0.6 \lesssim \alpha \lesssim 1.5$) having a large range of U_1, and found a practically identical generating function for Lα in all cases with $\tau_d(1215\text{ Å}) \gtrsim 0.3$. All seem to agree very well with the blackbody generating function (Fig. 2*c*), which is not surprising since in all these cases the fraction of neutral hydrogen is defined by the flux immediately beyond the Lyman edge, while the high-energy photons are not important. This is also the reason why we find no difference in $G(\tau)$ between dusty and dust-free cases for the blackbody ionizing continua. Some changes in $G(\tau)$ for Lα are seen in the power-law continuum case when $\tau_d(1215\text{ Å}) < 0.3$ [not large enough to destroy all Lα(coll)].

The other resonance lines of interest, those of C IV, O VI, Mg II, etc., are easier to treat, since they are formed by collisional excitation processes. Consider an ion with abundance N, and a line with emissivity $E(T_e)$, optical depth τ (thermal broadening), excitation energy E_{ij}, and a negligible probability of thermalization. Then,

$$G(\tau) \propto \frac{dE(T_e)}{d\tau} \propto \frac{NN_e \exp(-E_{ij}/kT_e)/\sqrt{T_e}}{N/\sqrt{T_e}} = N_e \exp(-E_{ij}/kT). \tag{15}$$

(If microturbulence is assumed instead, then we have to divide this expression by $T_e^{1/2}$, which will not significantly change our conclusion.) Generating functions for some typical cases are shown in Figure 2. Lines like C IV λ1549 or O VI λ1035, with high excitation temperature, show a typical behavior of $G(\tau)$: constant across the highly ionized H^+ zone, and sharp drop where the temperature starts to fall. This behavior is very insensitive to the amount of dust or its properties for dust/gas smaller than galactic, and produces a nearly uniform generating function (Fig. 2*f*). Some changes are seen in C IV λ1549 for large τ_d(912 Å) due to the very gradual decrease of temperature in this case (Fig. 2*g*). The Mg II λ2798 line is more sensitive to a change of parameters because of the large variation of N_e in its creation zone. The O VI generating function (not shown in Fig. 2) is practically uniform for all cases.

Another quantity needed for the calculations is the change of τ_d with τ_0 across the cloud which, for an ion N^{+i} with a relative abundance of N^{+i}/N, is

$$\frac{d\tau_d}{d\tau_0} \propto \frac{1}{(N^{+i}/N)}. \tag{16}$$

This can be derived from the ionization model calculations. If a collisionally excited line of the ion N^{+i} is the main coolant in its creation zone [which is the case for C^{+3} and to a fair approximation also for O^{+5}, Lα(coll), and Mg^{+1}], then the electron temperature is also defined by N^{+i}/N. In this case both $G(\tau)$ and $d\tau_d/d\tau_0$ depend on N^{+i}/N in such a way that their product is nearly uniform across the cloud. Since the relative number of photons destroyed by dust depends on $G(\tau)d\tau_d/d\tau_0$, we find that we can replace the calculated $G(\tau)$ and $d\tau_d/d\tau_0$ by two uniform functions. This was verified by comparing our *exact* $G(\tau)$ and $d\tau_d/d\tau_0$ with a uniform generating function case and found to be in very good agreement. Moreover, we found that all Lα destruction can be reduced to a single case, with the blackbody generating function (Fig. 2*c*) for $\tau_d(1215) < 0.3$ due to the role of Lα(coll) in cooling the transition zone, where it is created.

To summarize, the uniform generating function case is good for all metallic lines with and without dust. (Other lines for which a nearly uniform function was found are: Si IV λ1397, N V λ1240, C III λ977, etc., all with a considerable optical depth in the case of QSOs.) Lyman-α can be treated with a single generating function regardless of τ_d(eff). This suggests that our calculations are not very sensitive to the exact continuum shape or dust properties.

The optical depth in the different lines depends on U_1, and in some cases on τ_d, which in itself is a function of U_1. It will be shown later that the number of photons destroyed by dust is not very sensitive to τ_0, and its exact value is of secondary importance. The reader is referred to Baldwin and Netzer (1978) for more discussion of changes in T_e, emissivities, and ionization structure due to the presence of dust.

Destruction calculations have previously been reported by Panagia and Ranieri (1973*b*) and Bonilha, Ferch, and Salpeter (1979). The first is very different from what we considered here (small τ_0, and a simplified generating function), while the second investigated only cases of central generation, unlike the realistic nebulae discussed here. In general we find a qualitative agreement between many of our results and those given by Bonilha *et al.*

We have used our Monte Carlo program to calculate the destruction by dust of different lines. This is done by following the photon through the cloud and sampling for destruction between the successive scattering. It depends on the mean path traveled per scattering, and on τ_d(eff), and is thus different in different parts of the cloud. For instance, many core scatterings can be associated with only a short path and will therefore give less destruction than the much lower scattering in the wing. We have calculated cases with a large range of τ_0 and τ_d(eff), and several generating functions. They are summarized in Table 2 and Figures 6 and 7. Metallic lines are represented

TABLE 2

FRACTION OF ALL PHOTONS CREATED, THAT ARE DESTROYED BY DUST

A.

	Lα (Fig. 2*c*)		C IV λ1549 $\tau_0 = 2.2 \times 10^4$, UNIFORM GENERATION		
τ_d(eff)	Partial*	Complete	No Reflection	0.2 Reflection*	0.4 Reflection
0	0	...	0	0.48 (0)	...
0.01	0.14	0.09	0.04	0.52 (0.07)	...
0.03	0.31	...	0.21	0.57 (0.21)	0.52 (0.21)
0.1	0.61	0.47	0.44	0.75 (0.49)	...
0.3	0.75	0.69	0.66	0.83 (0.68)	0.81 (0.70)
1	0.87	0.9	0.85	0.93	...
3	0.95	...	0.96	0.97	...

B.

τ_d(eff) = 0.3, UNIFORM GENERATION

	COMPLETE REDISTRIBUTION		PARTIAL REDISTRIBUTION	
τ_0	No Reflection	0.2 Reflection	No Reflection	0.2 Reflection
10	0.41	...	0.37	...
10^2	0.54	0.81 (0.61)	0.50	0.80 (0.65)
10^3	0.68	0.83 (0.70)	0.67	0.84 (0.72)
10^4	0.53	0.77 (0.58)	0.65	0.83 (0.68)
10^5	0.41	...	0.70	...
10^6	0.35	...	0.59	...
10^7	0.41	...	0.65	...

NOTE.—In these calculations the gas optical depth τ_0 is held constant, and the dust optical depth varies by changing the dust/gas ratio.

* Considered to be the best estimate for realistic nebulae. Values in parentheses indicate destruction *inside* the cloud, for cases with reflection, while other numbers give the total destruction including the outer dust layer (see text). Table 2B is for scaling purposes, and ought to be used with Fig. 7 to estimate destruction in cases not shown in Table 2A. The quantity τ_d(eff) is the effective dust optical depth, to the point where 99% of the line photons were created. Estimated accuracy $\sim \pm 10\%$ for all numbers.

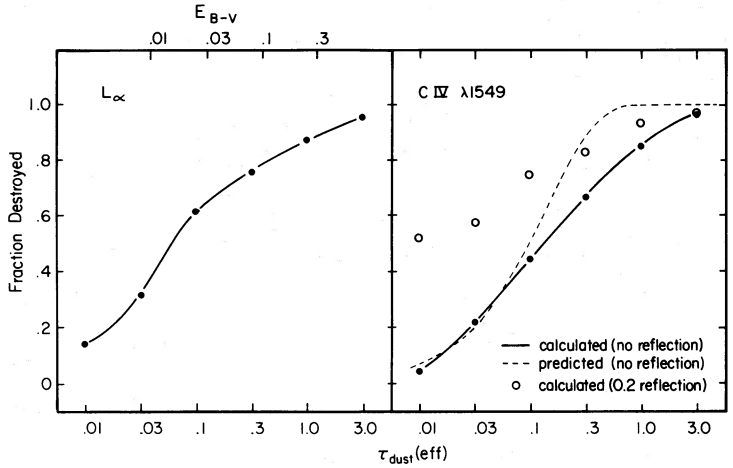

FIG. 6.—Destruction of Lα and C IV λ1549 due to internal dust. Partial redistribution assumed for both lines and the generating function for Lα is taken from Fig. 2*c*. E_{B-V} deduced assuming the interstellar extinction and albedo of 0.6. The C IV λ1549 has $\tau_0 = 2.2 \times 10^4$ and a uniform generating function. The calculated curve is for no reflection back by outer dust, while the more realistic case, with outer dust layer destroying photons going out, is shown with open circles. The predicted curve gives the destruction calculated from eq. (17) (no reflection case) using mean free path taken from a dust-free model. It overestimates the destruction since the mean path itself decreased in the presence of dust.

by a uniform generating function as discussed earlier. We also show the calculated E_{B-V} for the Lα case, assuming the interstellar extinction (Code *et al.* 1976) and albedo of 0.6. As seen in Figure 6, Lα destruction is nearly complete for $E_{B-V} \approx 0.1$.

As before, we assumed a forward scattering by the dust, which is justified since τ_0/τ_d is very large in all cases. However, the situation near the outer boundary of the slab is not as simple, due to the thick cool neutral layer, typical of our optically thick configuration. If the dust/gas ratio is the same everywhere, then the optical depth to dust beyond the H^+ zone is very large and can prevent any photons from escaping from that side. Photons traveling in this direction may be either destroyed or reflected back into the H^+ zone. Upon reflection, the photon may penetrate and escape from the inner, illuminated side (for nonresonance lines, mainly), or may be rescattered by the gas. The fractional number of photons reflected back into the H^+ zone depends both on $\bar{a}$ (the albedo) and $\bar{g}$ (the scattering angle), and our simple forward scattering treatment cannot hold any more. We have taken this into account by assuming a reflecting layer at the outer boundary of the H^+ zone, which reflects photons back with the same frequency, and a given probability. Using the observed interstellar dust properties (Lillie and Witt 1976), we considered cases with 0.2 and 0.4 reflection probability (the first is probably closer to the values of $\bar{g}$ observed). Note that in the 0.2 reflection case, 40% of *all* line photons are destroyed by dust while an *additional* destruction takes place for resonance lines. A comparision of the different reflection probability cases in Table 2

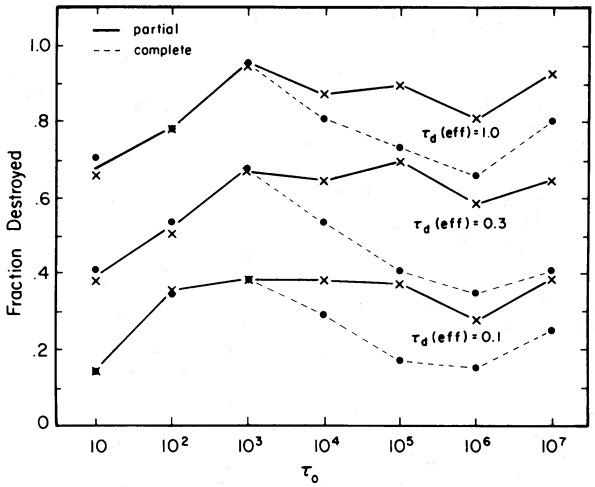

FIG. 7.—A scaling diagram for the two redistribution functions, uniform generation, and no reflection. The fractional destruction shown in Fig. 6 can be scaled to a different τ_0 by using the above curves. Cases with outer dust layer change more slowly, and can be obtained from Table 2.

suggests that they are nearly identical for large τ_0. This similarity arises because the gas optical depth is large enough to prevent a reflected photon from going all the way to the inner edge, so the photon is likely to be destroyed or reflected again toward the outer wall. This ensures a fair comparison of different resonance lines, regardless of the exact dust properties. On the other hand, the fractional destruction of the *nonresonance* lines depends strongly on the reflection probability, as they can easily pass through the ionized layer, provided τ_d(eff) is small enough. Hence the relative strength of resonance and nonresonance lines will depend strongly on the poorly known dust properties.

Lyman-α is different in this respect, due to its large optical depth in the cool partially neutral layer, which reflects back nearly all photons (less than 5% escaped in the outer direction in all cases tried). This causes less destruction by the outer dust. A similar, although less important, effect was found for Mg II λ2798. Note here that Lα destruction in density-bounded cases can be found using our calculations for the uniform case, with no reflection.

A theoretical destruction factor is calculated by:

$$F = 1 - \exp\left[-\frac{\langle P \rangle}{\tau_0}\,\tau_d(\text{eff})\right], \tag{17}$$

where the mean free path $\langle P \rangle$ is taken from the dust-free case (Fig. 1), and is independent of τ_d(eff). We compared F with actual calculations in Figure 6. Although the agreement is good for small τ_d(eff), the destruction is overestimated by (17) if τ_d(eff) > 0.1. The discrepancy is due to the decrease in the mean free path $\langle P \rangle$ in dusty cases, where photons travel a shorter distance than estimated from dust-free cases since the number of scatterings has been changed. This emphasizes the risk of using a simple extrapolation of a dust-free situation, to cases with dust.

Figure 7 is a scaling diagram to enable a comparison between cases of similar τ_d(eff) but different τ_0. The shape of the curves shown reflects the changes in the mean free path shown in Figure 1. Note that the scaling is computed for no reflection by outer dust, and one should use Table 2 if such a case is considered. (The dependence on τ_0 is much weaker in the 0.2 reflection case, where half or more of all resonance photons are destroyed in any event.)

b) Electron Scattering

A situation may arise where the optical depth of the slab to electron scattering becomes significant. Model ionization calculations for QSOs suggest that this is not important (best values of U_1 give H^+ column density less than 10^{22} cm^{-2} for thermal velocity), but it may be important in the early stages of nova outbursts (Ferland 1978*b*). A photon scattered by a free electron receives on the average a shift of $\sim$40 Doppler widths and can instantly escape. The opacity due to this process is linearly proportional to the H^+ column density; thus τ_e (the electron scattering optical depth) can be treated exactly as τ_d(eff) across the ionized zone. Our line destruction calculations can be applied to cases with large τ_e, using the results shown in Table 2 and Figures 6 and 7 (cases with no reflection).

We have looked in particular to the value of τ_e needed to alter significantly the mean number of scatterings in Lα. It was found to be around $\tau_e = 0.3$, with a large drop in $\langle N \rangle$ for larger values. This may look very large, but it is due to the fact the τ_e, like τ_d(eff), is extremely small in the region where most of the Lα scattering takes place, which is the partially neutral zone occupying only a small fraction of the cloud.

c) Thermalization

Line photons can be destroyed by thermalization (collisional de-excitation) in cases of high densities and large optical depths. For Lα the probability of this process is given by (8) to be $\sim 2 \times 10^{-17} N_e$ ($T_e \approx 10^4$ K). Cases of interest may be QSO emission regions where the density may approach 10^{10} cm^{-3}. The process was suggested by Krolik and McKee (1978) to explain the very small Lα/Hβ observed in 3C273. They found that if $N_e = 10^{10}$ cm^{-3} and $\tau_{L\alpha} \approx 5 \times 10^6$, it may be efficient enough to suppress Lα by a large factor. Their calculations were carried out using a mean escape probability technique, which assumes a uniform distribution of emitters. As noted here and also by Krolik and McKee, this is not the case for Lα in realistic situations, and the process ought to be calculated locally, considering the specific optical depth where each photon is created.

Our Monte Carlo program includes the destruction probability due to this process, and we have carried out calculations for two Lα generating functions. Results showing the fractional destruction at different electron densities are given in Figure 8. The cases chosen represent (i) a steep nonthermal continuum, a blackbody or a large U_1 flat continuum (Fig. 2*c*) and (*ii*) a flat nonthermal continuum with a small U_1 (Fig. 2*a*). The latter is probably close to the most extreme situation where photons penetrate deepest into the cloud (as far as $\tau_{L\alpha} = 10^7$) and the thermalization probability is close to its maximum. Most quasars known will fall between these two cases.

As seen, the amount of Lα thermalization is very small for $N_e \lesssim 10^{10}$ cm^{-3}. This is not surprising since only photons at very large optical depths are likely to be thermalized, and their relative number is small. Moreover, all photons created by recombination ($\sim$50% in most QSOs) are at optical depths of $\sim 10^5$ or less and can easily

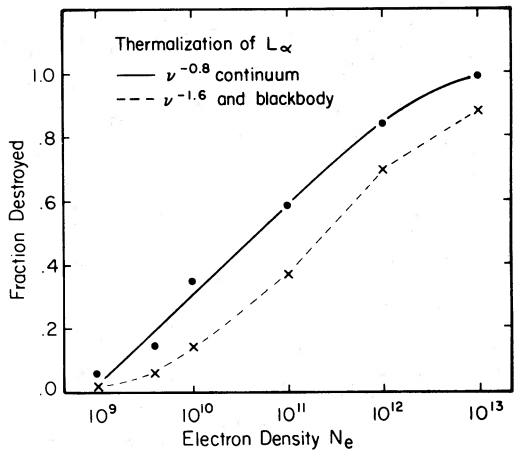

FIG. 8.—Destruction of Lα photons, due to thermalization (collisional de-excitation) as a function of electron density. The $\nu^{-0.8}$ continuum is the one from Fig. 2*a*, and represents an extreme case of large number of scatterings and deep penetration of photons. We assumed $q_{21} = 1.25 \times 10^{-8}$ cm^3 s^{-1}.

escape from the inner side of the cloud as long as $N_e < 10^{12}$ cm^{-3}. The ones that are more easily destroyed are those of Lα(coll). Semiforbidden lines observed in the spectrum of several QSOs indicate that a density of 10^{10} cm^{-3} is an upper limit (Baldwin and Netzer 1978) so that in the most extreme case only a fraction of Lα(coll) is destroyed and the recombination ratio Lα/Hβ ~ 35 cannot be reduced.

The thermalization fractions for $N_e \lesssim 10^{10}$ cm^{-3} can be approximated by

$$4 \times 10^4 \beta N_e/(1 + 4 \times 10^4 \beta N_e)\,, \tag{18}$$

where β is given in Table 1.

Nearly complete destruction is found for high densities of $N_e \gtrsim 10^{12}$ cm^{-3}, approaching the LTE limit. This may be related to a recent suggestion by Zirin (1978) that conditions in QSO clouds are similar to those in solar flares. One must realize, however, that if the hydrogen spectrum is due mainly to collisional processes, then the line emissivities change significantly (for instance, they are extremely sensitive to temperature fluctuations), and conditions are unlike those deduced by photoionization model calculations. In particular the relative strength of Lα (and also Hα) and the helium and metallic lines will be very different from what is calculated. That this is not observed, serves to reconfirm the upper limit on N_e in QSOs.

The thermalization probability for C IV λ1549 is much larger than that of Lα, but it is still not very significant within the range of optical depths ($\tau_0 \lesssim 5 \times 10^4$) and electron densities ($N_e < 10^{10}$ cm^{-3}) discussed here. We find that the destruction of C IV λ1549 photons is very uniform across the slab, in cases where thermalization is important. The change of the thermal structure in these cases is currently under study.

V. APPLICATIONS TO GASEOUS NEBULAE

a) Dust in QSOs

Several observed properties of QSOs may be related to the existence of dust. A well known one is the small Lα/Hβ observed in the spectrum of two objects (Davidsen, Fastie, and Hartig 1977; Hyland, Becklin, and Neugegauer 1978) and deduced, by comparison of low and high redshift QSOs, for many others (Baldwin 1977). A related point was mentioned by Baldwin and Netzer (1978), who showed that Lα, and perhaps also C IV λ1549 are suppressed by a factor of ~2 in the spectrum of several QSOs. These difficulties arise when comparing the observed and predicted (by photoionization) spectra.

We have tested the possibility that *internal* dust alters line intensities in QSOs, using our photoionization calculations, and the destruction probabilities given earlier. Some results are given in Table 3 where we take a ν^{-1} continuum and calculate the expected spectrum for solar abundances and different amounts of dust. U_1 is chosen to be slightly higher than needed in typical cases (Davidson 1977; Baldwin and Netzer 1978) so that models with small amounts of dust will give the best fit to an average QSO emission spectrum. The cases with dust are not a simple application of the destruction probability to the dust-free case, but involve recalculation of the ionization structure which is affected by the dust. We assumed the interstellar extinction curve and an albedo of 0.6 for all wavelengths and used this to calibrate τ_d(eff) for the different emission lines. The galactic dust/gas gives $\tau_d(1215) \approx 0.45$. Optical depth and region of creation for individual lines are taken from our model (see, for example, Fig. 3). Attenuation of nonresonance lines is deduced simply from the corresponding τ_d(eff) after allowing for 0.2 reflection by the outer dust (§ IV). More results for different conditions and small τ_d(eff) are given by Baldwin and Netzer (1978).

TABLE 3

SYNTHETIC QSO SPECTRUM

Line	No Dust	$\tau_d(1215) = 0.1$	$\tau_d(1215) = 0.45$	$\tau_d(1215) = 1$
Lα	100 (0.0)	100 (0.82)	100 (0.96)	100 (0.985)
C IV λ1549	72	54	35	18
C III λ1909	3.6	11.4	19	24
He II λ1640	3.4	9.1	15.5	20
O VI λ1035	16	12	5	1
Mg II λ2798	9.5	5.7	8.1	5.5
Hβ	1.3	3.4	7.5	9.7
τ(C IV λ1549)	9×10^4	1.0×10^4	3×10^3	1.4×10^3
τ(O VI λ1035)	8×10^3	3×10^3	7×10^2	2.7×10^2
dust/gas		0.1 × galactic	galactic	3 × galactic

NOTE.—$F_\nu \propto \nu^{-1}$, $U_1 = 8.7 \times 10^8$ cm s^{-1}, $N_e = 2 \times 10^9$ cm^{-3} at the inner face, solar abundances (Allen 1973). Relative line intensities shown for dust with the interstellar extinction, albedo of 0.6 for all wavelengths and 0.2 reflection probability (see text). Numbers in parentheses give total destruction of Lα relative to the dust-free case. Optical depth $\tau(H\beta) = 0$. Optical depth for C IV λ1549 and O VI λ1035 calculated assuming $V_{20} = 1$.

Table 3 reveals that Lα/Hβ decreases to a minimum value of ~10 for $\tau_d(1215) = 1$, which corresponds to $E_{B-V} \approx 0.25$. The line ratio cannot get much smaller since destruction of Hβ is getting important for such an amount of dust. Moreover, Hβ itself can have a nonnegligible optical depth, which will make Lα/Hβ larger. More important perhaps is the He II λ1640/Lα line ratio which exceeds its observed value for a dust/gas ratio galactic or higher. This line ratio is not sensitive to the particular model chosen, and gives a strong upper limit to the amount of dust in high-redshift QSOs. A comparison of Lα with many observed semiforbidden lines gives similar results and suggests again a rather small amount of internal dust. In addition, the total destruction of Lα exceeds 95% for a galactic dust/gas ratio, resulting in insufficient photons in the extrapolated continuum to give the commonly observed equivalent width of the line, even for a full coverage.

Table 3 and the other calculations carried for similar cases do not include complications due to the geometry of the emission region. These may include shadowing of some clouds by others (resulting in even smaller equivalent widths of Lα) and partial or complete obscuration of the central source. They may also involve the possibility of dust embedded in some clouds and not in others, a relatively thin neutral layer, etc. The main result, however, is that Lα and other resonance lines are getting too weak in comparison with the nonresonance lines. This is common to all cases.

To conclude, the observed He II λ1640 and Lα in many QSOs suggests that the amount of internal dust must be smaller than galactic. This does not depend very strongly on the assumed dust properties. It suggests that Lα/Hβ is not likely to drop below ~15 due to internal dust. We believe, therefore, that dust *around* QSOs may be more important, possibly having different properties from that in the interstellar medium. Reddening of all lines when passing through that dust may account for the Lα/Hβ observed, while the small amount and the different properties explain the continuum shape.

A point of interest is that our model, with reflecting dust layer at the outer edge, predicts an asymmetry in all line profiles if expansion or infall dominates over the emission region.

b) Balmer Optical Depth

The optical depth in Balmer lines can be deduced from our level-2 population and equations (9)–(12). This, however, gives the *total* optical depth, which is not particularly useful to infer observed properties like the Hα/Hβ ratio. The reason is that while most of the Hα creation takes place in the H^+ layer, most of the opacity is at the very edge of this zone, where the Lα trapping occurs. The average Hα photon thus encounters an optical depth much smaller than the total value calculated.

To find the mean Lα optical depth that corresponds to the mean Hα photon location, we calculate the quantity

$$\langle \tau_{L\alpha} \rangle = \int_0^{\tau_{L\alpha}} E(\tau)\tau d\tau \Big/ \int_0^{\tau_{L\alpha}} E(\tau) d\tau \,, \tag{19}$$

where $E(\tau)$ is the Hα emissivity. We find $\langle \tau_{L\alpha} \rangle \approx 3 \times 10^4$ for most power-law continua and $\langle \tau_{L\alpha} \rangle \approx 2 \times 10^4$ for blackbodies (if thermal velocity is assumed, then the number will be ~1.5 times larger). Optical depths twice as large will be taken to account for the zero escape probability of Lα through the outer side. The location found is about halfway through the slab, and we have used the corresponding number of scattering taken from our Figure 1 to deduce an "effective optical depth" for Hα, in the same way as in (9). The result is an effective $\tau_{H\alpha}$ smaller by a factor of about 8 for blackbodies, and by a factor of about 15 for flat power laws, than the one deduced from Table 1. The very large factor suggests that nearly all the Hα opacity is toward the outer side and photons stand little chance of escaping from this direction. The number of scatterings of Hα photons deduced from $\tau_{H\alpha}$(eff)

agrees well with the *median* number of scattering of Hα and is the one to use when a "mean escape probability" approach is used. Such an approach was chosen, for instance, by Netzer (1975, 1977) and Krolik and McKee (1978) to investigate the Balmer decrement in active galactic nuclei, and a good representation of the average conditions is essential there. Our discussion, of a simple nova shell, shows that consistent results are obtained with this effective $\tau_{H\alpha}$ (see Appendix).

A point to note is that the mean escape probability of the average Hα photon is smaller than that deduced from $\tau_{H\alpha}$(eff), due to the small probability of escaping toward the outer edge. Therefore, a somewhat higher $\tau_{H\alpha}$ should be used in large optical depth situations. Another point is that $\tau_{H\alpha}$(eff) is practically decoupled from $\tau_{L\alpha}$ (which is independent of the flux), and can be used as a free parameter in such calculations.

c) *Collisional Excitation of Balmer Lines*

Perhaps the most important effect which cannot be taken into account in this "average Balmer photon" approach is the collisional excitation process ($2 \rightarrow 4$) which can be significant (Netzer 1977; Krolik and McKee 1978), but, as indicated by our calculation, only deep in the cloud, where most of level-2 population occurs and where recombination is negligible. Very deep in the cloud, for instance, one should expect the efficiency of this process to be up to 15 times larger than for the average photon. We can estimate this as follows: the recombination contribution to Hβ is proportional to the number of ionizing photons $Q(\mathrm{H})$, and the collisional contribution is proportional to the *column density of level-2 population*, N_2, which is given by $\tau_{H\alpha}/K_{H\alpha}$; therefore,

$$\frac{H\beta(\mathrm{coll}, 2 \rightarrow 4)}{H\beta(\mathrm{recb})} = \left[\left(\frac{\tau_{H\alpha}}{K\alpha}\right) q_{24} N_e\right] \Big/ \left[\frac{Q(\mathrm{H})}{4\pi r^2} \frac{\alpha^{\mathrm{eff}}(H\beta)}{\alpha^{\mathrm{eff}}(L\alpha)}\right] \approx \left[\frac{\eta\beta}{K\alpha} \frac{Q(\mathrm{H})}{4\pi r^2} q_{24} N_e\right] \Big/ \left[\frac{Q(\mathrm{H})}{4\pi r^2} \times 0.115\right]$$

$$\approx 1.1 \times 10^{-10} N_e\,, \tag{20}$$

where in the second step we used our expression for $\tau_{H\alpha}$ deduced in equations (9)–(12) and in the third we have assumed $q_{24} = 3.2 \times 10^{-9} (T_e = 10^4)$, typical of the region beyond the recombination zone for power-law continua; q_{24} form Krolik and McKee (1978) weighted to include conversion to Pα, $\eta = 2$, and $\beta = 6.6 \times 10^{-16}$. If $N_e \approx 10^{10}$ cm^{-3}, then collisional contribution equals recombination. Because of the larger efficiency of exciting Hα, and because of the efficient conversion of Hβ photons into Hα via self-absorption deep in the cloud, we estimate that at these densities Hα/Hβ > 10 unless $\tau_{H\alpha}$ is extremely large. This ratio is higher than observed in most Seyferts or QSOs (Baldwin 1975; Osterbrock 1977) and therefore $N_e \approx 10^{10}$ cm^{-3} seems to be an upper limit on the electron density. This upper limit is in fact identical to the one mentioned earlier from consideration of the strength of semiforbidden lines.

Until a complete solution of the Balmer transfer is available, we suggest that recombination and collisional excitation be calculated *separately*, each with its corresponding $\tau_{H\alpha}$ (the one for collisional excitation is practically the total $\tau_{H\alpha}$, while the one for recombination about 10% of it), and the results added together according to equation (20). Note also that the calculated N_2 deep in the cloud is subject to larger uncertainties due to the nonnegligible transition rate to upper levels. We find, however, that this is not severe unless the density is very high.

Finally, if turbulent velocity is different from the 20 km s^{-1} assumed here, one should scale $\tau_{H\alpha}$ accordingly by using a factor of $(20/V)^2$ where V is in km s^{-1}. This takes into account both the change in opacity of Hα and the change in the mean number of scatterings of Lα.

d) *Level-2 Ionization and Two-Photon Emission*

If there is a large column density of hydrogen atoms in the first excited state, a nebula can be optically thick to photoionization in the Balmer continuum (Kirshner and Kwan 1975; Strittmatter *et al.* 1977). At even large column densities, the nebula could be optically thick at λ = 1215 Å and the process $L\alpha + L\alpha + H^0 \rightarrow H^+ + e^- \rightarrow H^0 + L\alpha + h\nu$ may be important. We can calculate this effect by comparing the total optical depth deduced earlier for Hα, with the one for the continuum at different wavelengths. Taking the level-2 photoabsorption cross section in Allen (1973), we get

$$\frac{\tau(\lambda 1215, \mathrm{continuum})}{\tau_{H\alpha}} \approx 2 \times 10^{-6}\,. \tag{21}$$

Taking into account an efficiency factor of ~2 due to the increase of the mean free path of the Lα photon, we find that the process cannot be important for $\tau_{H\alpha} \lesssim 5 \times 10^4$. Using an approach similar to the one in § III, we can write this as

$$\tau_{L\alpha \rightarrow H^+} \approx 1.4 \times 10^{-21} \frac{Q(\mathrm{H})}{4\pi r^2}\,. \tag{22}$$

It is possible that this process is important in QSOs, where $\tau_{H\alpha}$ may become extremely large. However, if any

Lα destruction occurs due to this, it must be where $\tau_{L\alpha}$ is very large which is the region with very little recombination. The loss of Lα photons cannot therefore be significant (see discussion of thermalization in § IV).

Using the level-2 column density N_2, we can deduce the relative intensity of the two-photon continuum. In high-density situations $n(2s)/n(2p) = \frac{1}{3}$, therefore,

$$\frac{N(2\text{ photons})}{N(L_\alpha)} = \frac{0.25\,A(2\text{ photons}) \times N_2}{\eta Q(\mathrm{H})/4\pi r^2} = \frac{2.06 \times \tau_{H\alpha}/K\alpha}{\eta Q(\mathrm{H})/4\pi r^2} = 6.5 \times 10^{12}\beta\,, \tag{23}$$

where in the last step we have made use of $\tau_{H\alpha} = \eta\beta Q(\mathrm{H})/4\pi r^2$.

Even with the largest β given in Table 1, the above does not amount to more than $\sim 1\%$.

VI. CONCLUSIONS

Realistic models of the ionization structure of photoionized nebulae have been combined with the Monte Carlo line transfer technique to study resonance line transfer and the effects of line trapping. Although the bulk of the work concerns Lα, several other lines which are important coolants in gaseous nebulae were also considered.

The presence of very large Lα optical depths in the outer transition zone of radiation-bound nebulae greatly increases the amount of Lα trapping and level-2 population. Although few photons were created here, many photons which were originally created at much smaller optical depths are scattered into this region. Collisional excitation of Lα is important in the transition zone for power-law continua, and this further increases the level-2 population. As a result, we find that $\tau_{H\alpha}$ is greatly concentrated deep in the cloud, a situation resembling somewhat the Lα opacity. We give simple formulae relating $\tau_{H\alpha}$ to the incident ionizing photon flux, and show that an effective optical depth 8–15 times smaller must be used in mean escape probability calculations. In the Appendix we demonstrate that this $\tau_{H\alpha}$(eff) can successfully account for both the Balmer decrement and the O I λ8446 fluroescence in the nova V1500 Cygni.

We find, by comparing the $(2 \rightarrow 4)$ collisional contribution to Hβ, with the recombination one, that the first can be significant for high densities. This indicates that the observed Hα/Hβ in active nuclei is inconsistent with $N_e > 10^{10}$ cm^{-3}. Related to this is the possibility of collisionally de-exciting Lα, under conditions of large optical depth. We have calculated this with our Monte Carlo program, and found that the process cannot be significant under the densities assumed. We conclude that the anomalously high Hβ/Lα in some QSOs cannot be accounted for by thermalization of Lα if $N_e \lesssim 10^{10}$ cm^{-3}.

Finally, the effects of dust have been included in both the ionization structure and line transfer. Dust is an extremely efficient mechanism for destroying Lα; for example, we found that nearly all Lα photons are destroyed when $E_{B-V} \approx 0.1$. We show that the uniform-generation case gives adequate representation of most metallic lines, and that a single Lα generating function can be used in all dusty models. Simple scaling curves are given for computing destruction probabilities for various lines, and for a wide range of τ_{dust}. Dust will affect ratios of forbidden and semiforbidden line intensities to permitted line intensities, so these ratios provide a great deal of information on the dust content of emission line regions. Synthetic QSO emission line spectra have been computed with various values of the dust-to-gas ratio, and comparison with observations shows that this ratio must be less than the galactic value in most objects. Although some Lα destruction may be important, it seems not to be enough to explain the too small observed Lα/Hβ in some cases.

The final version of this paper has been improved due to comments by R. London, J. Krolik, and others, for which we are grateful.

APPENDIX

a) Hα/Hβ *and* O I λ*8446 in Nova Cygni*

Balmer decrements of novae during the nebular phase have long been known to deviate from case B predictions in a time-dependent manner (Payne-Gaposchkin 1957; Meinel 1963; Ferland 1978*a*). This has been attributed to variable Balmer self-absorption (Ferland 1978*a*). The evolution of a typical nova Balmer decrement can be characterized as follows (only Hα/Hβ can be measured without problems with line blending): Initially the Balmer decrement is slightly flatter than case B predictions (Hα/Hβ ∼ 2.2). Within a few weeks the decrement becomes quite steep (Hα/Hβ ∼ 6). As the decrement grows steeper, the intensity of O I λ8446 increases and the violet side of emission lines is attenuated. Over the next few hundred days the Balmer decrement slowly approaches case B, O I λ8446 subsides, and the emission line profiles become more symmetric.

Strittmatter *et al.* (1977) first proposed that emission lines of V1500 Cygni were quite optically thick, but their analysis of the line transfer processes is inconsistent with our previous discussion. The Hα optical depth can be computed under our assumptions with the optical data of Ferland, Lambert, and Woodman (1979, in preparation). The Balmer decrement was steepest on ∼day 20.6 [Hα/Hβ ≈ 6, $F(\mathrm{H}\beta) = 10^{-8.87}$ ergs s^{-1} cm^{-2}]. A distance of 1.8 kpc and an interstellar reddening of $E_{B-V} = 0.53$ will be assumed (Ferland 1977). If the covering factor is

$\sim\frac{1}{2}$, then $Q(\mathrm{H}) \approx 10^{49.12}$ photons s^{-1}. The expansion velocity is ~ 2000 km s^{-1} (Tomkin, Woodman, and Lambert 1976), so $r \approx 10^{14.6}$ cm. Equation (9) predicts $\tau_{\mathrm{H}\alpha} \approx 4400$. The "effective" optical depth (for comparison with mean escape probability calculations) is 8 times smaller (see above). Tomkin, Woodman, and Lambert (1976) set an upper limit to the turbulent velocity of 80 km s^{-1} (from the Bowen O III lines), so we take $V_{\mathrm{turb}} \sim 40$ km s^{-1}. The value for comparison with models will be therefore $\tau_{\mathrm{H}\alpha}(\mathrm{eff}) \approx 140$.

As the outburst progresses, $\tau_{\mathrm{L}\alpha}$ will remain constant (if turbulence is constant and the nebula remains radiation bounded) but $\tau_{\mathrm{H}\alpha}$ will decrease rapidly [Since $Q(\mathrm{H})$ falls and r^2 increases] and the nova should follow an arc in the $\mathrm{H}\alpha/\mathrm{H}\beta/\mathrm{H}\gamma$ plane (Netzer 1975).

The steepest value observed by Ferland, Netzer, and Shields (1979) of $\mathrm{H}\alpha/\mathrm{H}\beta \sim 6$ is very close to the steepest ratio calculated by Netzer (1975) for $\tau_{\mathrm{L}\alpha} \approx 4 \times 10^4$, as was verified by interpolating his results and also by a similar set of calculations carried for the above condition, using the same computer program. The corresponding $\tau_{\mathrm{H}\alpha}$ is about ~ 100.[1] Regarding the degree of approximation in the calculation, and the uncertainties in deducing distance, covering factor, and turbulences for the nova, we believe this to be in good agreement with our empirical $\tau_{\mathrm{H}\alpha}$. The violet/red emission line asymmetry is caused by the different distributions of the Balmer line generating function and level-2 population (see above, and Ferland, Netzer, and Shields 1979).

The largest O I λ8446/Hα ratio observed was 0.3 and can be compared with Netzer and Penston (1976) to find a third estimate of $\tau_{\mathrm{H}\alpha}$. After dividing the intensity ratio by 20 to account for the enhanced oxygen abundance (Ferland and Shields 1978) and using our value of $\langle N \rangle$, we find $\tau_{\mathrm{H}\alpha} \approx 320$. The three measurements of $\tau_{\mathrm{H}\alpha}[\mathrm{H}\alpha/\mathrm{H}\beta]$, $\eta\beta Q(\mathrm{H})$ from equations (9)–(12) corrected for the effective $\tau_{\mathrm{H}\alpha}$, and O I λ8446/Hα, agree thus within a factor of ~ 3. It is not surprising, in fact, that the value deduced from the O I λ8446/Hα is the largest, since the conversion of Lβ photons is most effective near the neutral zone, where both $\tau_{\mathrm{H}\alpha}$ and the abundance of O I reach their maximum. This high efficiency may be interpreted as a larger $\tau_{\mathrm{H}\alpha}(\mathrm{eff})$ than actually exists. Another uncertainty is the high conversion probability for the large abundance case which affects the escape of Lβ photons through providing another channel for their destruction. Our discussion of the level-2 ionization by Lα, and the results shown in (21) and (22), indicate that this must have negligible influence on the ionization structure of nova V1500 Cygni after day ~ 5.

b) Dust Heating

Infrared emission characteristic of a 500–1500 K blackbody radiation is often observed from photoionized nebulae (e.g., Osterbrock 1974). This emission is believed to be caused by reradiation of energy absorbed by dust. Destruction of both Lα and continuum photons may contribute to the grain heating (Aannestad 1978). In this section our calculations of the Lα destruction efficiency are combined with standard interstellar reddening curves (Code *et al.* 1976) to determine the relative importance of the two heating processes.

A constant dust albedo of 0.6 will be assumed, and the effective dust optical depth computed as above. Blackbody radiators were assumed with temperature T_*. The ratio of the continuum to Lα heating

$$R = \frac{\int_{912}^{\infty} \{1 - \exp\,[\tau_d(\mathrm{eff})]\} B_\lambda d_\lambda}{eQ(\mathrm{H})h\nu_{1215}} \tag{24}$$

[1] Note that the values given in Netzer (1975) are for optical depth measured at the *slab center*.

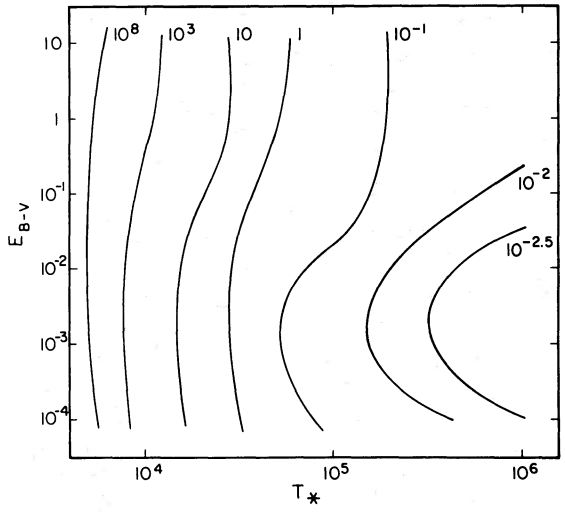

FIG. 9.—Ratio of continuum (0.912–2 μm) to Lα grain heating as a function of the central blackbody temperature T_*. Standard reddening curves (Code *et al.* 1976) and a constant albedo of 0.6 were assumed. Lα destruction efficiency was taken from our Monte Carlo calculations.

(e is an efficiency factor for Lα destruction as calculated previously) was computed numerically. Lα photons escaping from the inner boundary of the nebula were allowed to escape freely, which is equivalent to assuming that the nebulae covering factor is small so that a second encounter with a dusty region is unlikely.

Figure 9 shows lines of constant R in the (T_*, E_{B-V})-plane. The relative importance of the two heating mechanisms is determined mainly by T_* since Q(H) increases much more rapidly with increasing T_* than does the energy in the Balmer continuum. Continuum heating clearly dominates if $T_* < 10^{4.6}$ K.

A contour plot similar to Figure 9 has also been computed for power-law radiation $F_\nu \propto \nu^{-\alpha}$. R lies within the range $10^{0\pm1}$ for $0.5 < \alpha < 2$, and is mainly determined by the reddening. Continuum heating equals Lα heating for $E_{B-V} \approx 0.1$ when $\alpha \approx 1$.

Galactic novae of the DQ Her type are observed to undergo a rapid drop in visual luminosity with a commensurate increase in infrared luminosity (Hyland and Neugebaur 1970; Geisel, Kleinmann, and Low 1970). This drop is believed to mark an epoch of rapid grain formation (Ney and Hatfield 1978). The central object temperature is poorly determined during this phase of the nova outburst, but $T_* \lesssim 50{,}000$ K is reasonable since He II lines are not present. Figure 9 shows that continuum heating is competitive with Lα heating at this temperature and should be considered when modeling this phase of the outburst. Continuum heating may dominate since the dust must be heated as soon as it becomes optically thick to visual radiation (the visual drop and infrared excess are strongly correlated). The neutral material beyond the H^+ Strömgren sphere is an amenable site for grain formation (Gallagher 1977), but this region is well shielded from both Lα and Lyman continuum photons, so only Balmer continuum radiation may be effective.

REFERENCES

Aannestad, P. A. 1975, *Ap. J.*, **200**, 30.
———. 1978, *Ap. J.*, **220**, 538.
Adams, T. F. 1972, *Ap. J.*, **174**, 439.
Allen, C. W. 1973, *Astrophysical Quantities* (London: Athlone Press).
Auer, L. H. 1968, *Ap. J.*, **153**, 783.
Avery, L. W., and House, L. L. 1968, *Ap. J.*, **152**, 493.
Baldwin, J. A. 1975, *Ap. J.*, **201**, 26.
———. 1977, *M.N.R.A.S.*, **178**, 67p.
Baldwin, J. A., and Netzer, H. 1978, *Ap. J.*, **226**, 1.
Bonilha, J. R. M., Ferch, R., and Salpeter, E. E. 1979 *Ap. J.*, in press.
Chaisson, E. J., Lichten, S. M., and Rodriguez, L. F. 1978, *Ap. J.*, **221**, 810.
Code, A. D., Davis, J., Bless, R. C., and Brown, R. H. 1976, *Ap. J.*, **203**, 417.
Davidsen, A. F., Fastie, W. G., and Hartig, G. F. 1977, *Nature*, **269**, 203.
Davidson, K. 1977, *Ap. J.*, **218**, 20.
Ferland, G. J. 1977, *Ap. J.*, **215**, 873.
———. 1978*a*, *Ap. J.*, **219**, 589.
———. 1978*b*, Ph.D. thesis, University of Texas at Austin.
Ferland, G. J., Netzer, H., and Shields, G. A. 1979 *Ap. J.* (in press).
Ferland, G. J., and Shields, G. A., 1978, *Ap. J.*, **226**, 172.
Gallagher, J. S. 1977, *A.J.*, **82**, 209.
Geisel, S. L., Kleinmann, D. E., and Low, F. 1970, *Ap. J. (Letters)*, **161**, L101.
Hummer, D. G., and Rybicki, G. B. 1971, *Ann. Rev. Astr. Ap.*, **9**, 273.
Hyland, A. R., Becklin, E. E., and Neugebaur, G. 1978, *Ap. J. (Letters)*, **220**, L73.
Hyland, A. R., and Neugebauer, G. 1970, *Ap. J. (Letters)*, **160**, L177.
Jefferies, J. T. 1968, *Spectral Line Formation* (Waltham: Blaisdell).
Kirshner, R. P., and Kwan, J. 1975, *Ap. J.*, **197**, 415.
Krolik, J. H., and McKee, C. F. 1978, *Ap. J.*, **223**, 702.
Lillie, C. F., and Witt, A. N. 1976, *Ap. J.*, **208**, 64.
Mathis, J. S., Rumple, W., and Nordsieck, K. H. 1977, *Ap. J.*, **217**, 425.
Meinel, A. B. 1963, *Ap. J.*, **137**, 834.
Mezger, P. G., Smith, L. F., and Churchwell, E. 1974, *Astr. Ap.*, **32**, 269.
Mihalas, D. 1970, *Stellar Atmospheres* (San Francisco: Freeman).
Netzer, H. 1975, *M.N.R.A.S.*, **171**, 395.
———. 1977, *M.N.R.A.S.*, **178**, 489.
Netzer, H., and Penston, M. V. 1976, *M.N.R.A.S.*, **174**, 319.
Ney, E. P., and Hatfield, B. F. 1978, *Ap. J. (Letters)*, **219**, L111.
Osterbrock, D. E. 1962, *Ap. J.*, **135**, 195.
———. 1974, *Astrophysics of Gaseous Nebulae* (San Francisco: Freeman).
———. 1977, *Ap. J.*, **215**, 733.
Panagia, N., and Ranieri, M. 1973*a*, *Astr. Ap.*, **24**, 219.
———. 1973*b*, *Mém. Soc. Roy. Liège*, Ser. 6, **5**, 275.
Payne-Gaposchkin, C. 1957, *The Galactic Novae* (Amsterdam: North-Holland).
Spitzer, L. 1944, *Ap. J.*, **99**, 1.
Strittmatter, P. A., *et al.* 1977, *Ap. J.*, **216**, 23.
Tomkin, J., Woodman, J., and Lambert, D. L. 1976, *Astr. Ap.* **118**, 319.
Unno, W. 1952, *Pub. Astr. Soc. Japan*, **4**, 100.
Zirin, H. 1978, *Ap. J. (Letters)*, **222**, L105.

GARY FERLAND: Institute of Astronomy, Madingley Rd., Cambridge, CB3 0HA, England

HAGAI NETZER: Department of Astronomy, University of Texas, Austin, TX 78712